Project COMET:

Search for coherent neutrino-less μ -e conversion at J-PARC

(JINR participation)

Report on the project and proposal for its extension

DLNP: V. N. Duginov, K. I. Gritsai, I. L. Evtoukhovich, P.G. Evtoukhovich, V.A. Kalinnikov, X. Khubashvili, E. M. Kulish, A.S. Moiseenko, B. M. Sabirov, A. G. Samartsev, Yu.Yu.Stepanenko, Z. Tsamalaidze, N. Tsverava, E. P. Velicheva, A. D. Volkov

VBLPHE: V.V. Elsha, T. L. Enik, S. A. Movchan, S. N. Shkarovskiy

BLTP: Sh. Bilanishvili, G. A. Kozlov

LIT: G. Adamov, T. Javakhishvili, A. Khvedelidze

Project leader Z.Tsamalaidze

The COMET project at JINR has been approved by the JINR PAC on nuclear physics in 2014 for the period 2014-2016. Below the results of the activity will be presented and the extension of the project for 2017-2019 years will be proposed.

1.Introduction

COMET (COherent Muon to Electron Transition) is the experiment [1] at J-PARC to search for coherent neutrino-less conversion of muons to electrons $\mu^- \rightarrow e^-$ in the presence of a nucleus, $\mu^- + N(A,Z) \rightarrow e^- + N(A,Z)$, with a single event sensitivity $\mathrm{Br}(\mu^- N \rightarrow e^- N) \sim 10^{-17}$.

Flavor transitions between the charged leptons (Charged Lepton Flavor Violation, CLFV) have a great potential to reveal new physics phenomena beyond the Standard Model (SM). Many models of such physics require the existence of CLFV at the level that is accessible in future experiments.

Muons provide the best laboratory to study CLFV as they can be produced in substantial numbers and have a sufficiently long lifetime. Present accelerators can produce about 10^{15} muons/year, and it is anticipated that it will be possible to produce 10^{18} - 10^{19} muons/year with a new high intensity source that is proposed in conjunction with the main J-PARC proton synchrotron ring.

Within the SM, the expected branching ratio of μ - e conversion is less than 10^{-54} what is beyond the experiment's reach. Therefore, any observation of $\mu^- \rightarrow e^-$ conversion would be a clear signal of a new physics beyond the SM. A measurement at the level of $< 10^{-16}$ for $\mu^- \rightarrow e^-$ conversion, which is the COMET goal, is a factor of 10,000 better than the current experimental limit.

COMET will use a bunched proton beam slow-extracted from the J-PARC Main Ring. Beam bunching is necessary to reject beam-related backgrounds. The experimental setup consists of high magnetic field solenoids for pion capture, C-shaped curved solenoids with momentum selection, and a C-shaped curved solenoid spectrometer. The experiment will require about 2×10^{18} stopping muons, which, with the expected transmission of muons in the muon beam line, will require about 8.5×10^{20} protons of 8 GeV energy.

In the chapters that follow, the physics motivation and method of observation are presented, together with the experiment layout, status of the experiment and preliminary schedule. The JINR contribution is described in detail.

2. Physics motivation

The charged lepton flavor violation (CLFV) processes attract much attention from both theoretical and experimental points of views. The search for CLFV processes has notable advantages, including the following: (1) CLFV can have sizable contributions from new physics and thus can manifest themselves in future experiments; (2) CLFV does not have any sizable contribution from the SM which would limit the experimental sensitivity to search for new physics.

Although CLFV has never been observed, LFV among neutrino species has been experimentally confirmed with the discovery of neutrino oscillations [2, 3], and hence lepton flavor conservation is now known to be violated. The phenomenon of oscillation means that neutrinos are massive and hence the SM must be modified so that LFV can occur.

It is well known that in the minimally extended SM which takes into account the neutrino oscillations, the predicted branching ratios for CLFV are too small to be observed. For example, the prediction for the Br($\mu \rightarrow e\gamma$) is < 10^{-54} [4-7].

The new physics beyond the SM predict CLFV at some level. Examples of such new physics models are multiple and include, in particular, supersymmetric (SUSY), extra dimension, little Higgs models, models with new extra gauge Z' bosons, with new heavy leptons, lepto-quarks etc. (see, for example [8-19]). Each model has its own predictions for relative probabilities of the CLFV processes including $\mu^- + N \rightarrow e^- + N$, and the predicted branching ratios are within the COMET reach.

2.1 $\mu^- \rightarrow e^-$ conversion

One of the most prominent muon LFV processes is coherent neutrino-less conversion of muons to electrons ($\mu^- \rightarrow e^-$ conversion). Once a negative muon is stopped by some material, it is trapped by an atom, and a muonic atom is formed. After it cascades down energy levels in the muonic atom, the muon is bound in its 1*s* ground state. The fate of the muon is then to either decay in orbit ($\mu^- \rightarrow e^- \nu_\mu \bar{\nu}_e$) or be captured by a nucleus of mass number *A* and atomic number *Z*, namely, $\mu^- + N(A,Z) \rightarrow \nu_\mu + N(A,Z-1)$. However, in the context of physics beyond the SM, the exotic process of neutrino-less muon capture, such as

$$\mu^- + N(A,Z) \rightarrow e^- + N(A,Z) \qquad (2.2)$$

is also expected, called $\mu^- \rightarrow e^-$ conversion in a muonic atom. This process violates the conservation of lepton flavor numbers, L_e and L_μ, by one unit, while the total lepton number *L* is conserved. The final state of the nucleus (*A*, *Z*) could be either the ground state or one of the excited states. In general, the transition to the ground state, which is called coherent capture, is dominant. The rate of the coherent capture over non-coherent capture is enhanced by a factor approximately equal to the number of nucleons in the nucleus, since all the nucleons participate in the process.

2.2 $\mu^- \rightarrow e^-$ conversion vs $\mu^+ \rightarrow e^+\gamma$ and $\mu^+ \rightarrow e^+e^+e^-$

Apart from $\mu^- \rightarrow e^-$ conversion, there might be two other CLFV processes: muon decays $\mu \rightarrow e\gamma$ and $\mu \rightarrow eee$.

Two possible contributions in the $\mu^- \rightarrow e^-$ transition diagrams have been considered in [20]. One of them is a photonic contribution, and the other one is a non-photonic contribution. For the photonic contribution, there is a definite relation between the $\mu^- \rightarrow e^-$ conversion process and the $\mu^+ \rightarrow e^+\gamma$ decay. Suppose the photonic contribution dominates, then the branching ratio of the $\mu^- \rightarrow e^-$ conversion process is expected being smaller than that of $\mu^+ \rightarrow e^+\gamma$ decay due to electromagnetic interaction of a virtual photon. This implies that the search for $\mu^- \rightarrow e^-$ conversion at the level of 10^{-16} is comparable to that of $\mu^+ \rightarrow e^+\gamma$ at the level of 10^{-14}.

If the non-photonic contribution dominates, the $\mu^+ \rightarrow e^+\gamma$ decay would be small whereas the $\mu^- \rightarrow e^-$ conversion could be sufficiently large to be observed. It is worth noting the following. If a $\mu^+ \rightarrow e^+\gamma$ signal is found, the $\mu^- \rightarrow e^-$ conversion signal should also be found. A ratio of the branching ratios between $\mu^+ \rightarrow e^+\gamma$ and $\mu^- \rightarrow e^-$ carries vital information on the intrinsic

physics process. If no $\mu^+ \rightarrow e^+\gamma$ signal is found, there will still be an opportunity to find a $\mu^- \rightarrow e^-$ conversion signal because of the potential existence of non-photonic contributions.

Like for the $\mu^- \rightarrow e^-$ conversion, sensitivity of the $\mu^+ \rightarrow e^+e^+e^-$ process is also 2 orders of magnitude less than that of $\mu^+ \rightarrow e^+\gamma$, therefore 10^{-16} for $\mu^+ \rightarrow e^+e^+e^-$ (what is the aim of the "Mu3e" Proposal in PSI) is equivalent to 10^{-14} for $\mu^+ \rightarrow e^+\gamma$. But the diagrams describing these muon decays are different, therefore all three CLFV processes are differently sensitive to various BSM models. Hence, the experiments on search for $\mu^- \rightarrow e^-$ conversion, $\mu^+ \rightarrow e^+\gamma$ and $\mu^+ \rightarrow e^+e^+e$ are complimentary.

In Table 2.1 one can see the current and planned limits for the three CLFV processes with muons.

Table 2.1: experimental limits for the CLFV processes.

process	current limit	plan
$\mu \rightarrow e\gamma$	< 4.3 x 10^{-13} (MEG, 2016)	< 5.0 x 10^{-14} (MEG-II, PSI)
$\mu \rightarrow eee$	< 1.0 x 10^{-12} (SINDRUM, 1988)	~ 10^{-16} (Mu3e Proposal, PSI)
$\mu N \rightarrow eN$	< 7.0 x 10^{-13} (SINDRUM-II, 2006)	< $10^{-16\text{-}17}$ (**COMET**, J-PARC and Mu2e, FNAL)

The three CLFV processes have different experimental issues that need to be solved to realize improved experimental sensitivities. They are summarized in Table 2.2. The processes $\mu^+ \rightarrow e^+\gamma$ and $\mu^+ \rightarrow e^+e^+e^-$ are detector-limited. To go beyond the present sensitivities, the resolutions of the detectors have to be improved, which is, in general, very hard problem. On the other hand, for $\mu^- \rightarrow e^-$ conversion, there are no accidental background events, and an experiment with higher rates can be performed.

Table 2.2: CLFV processes and issues.

Process	Major backgrounds	Beam	Sensitivity Issues
$\mu^+ \rightarrow e^+\gamma$	accidental	DC beam	detector resolution
$\mu^+ \rightarrow e^+e^+e^-$	accidental	DC beam	detector resolution
$\mu^- \rightarrow e^-$ conversion	beam-associated	pulsed beam	beam qualities

Note, that over the past 30 years the experimental upper limits have been improved by 5 orders of magnitude. The latest search for $\mu^- \rightarrow e^-$ conversion was performed by the SINDRUM-II collaboration at PSI. They set the current upper limit on $B(\mu^- + Au \rightarrow e^- + Au) < 7 \times 10^{-13}$ [21].

2.3. Signal and background events

The event signature of coherent $\mu^- \rightarrow e^-$ conversion in muonic atom is emission of a mono-energetic single electron with an energy $E_e \approx m_\mu - B_\mu$ where m_μ is the muon mass and B_μ is the binding energy of the 1*s* muonic atom. Due to smallness of B_μ, E_e is close to m_μ.

From an experimental point of view, $\mu^- \rightarrow e^-$ conversion is very attractive process. First, the electron energy of about 105 MeV is far above the end-point energy of the muon decay spectrum ($\sim$ 52.8 MeV). Second, since the event signature is a mono-energetic electron, no coincidence measurement is required. The search for this process has the potential to improve sensitivity by using a high muon rate without suffering from accidental background events, which would be serious for other processes, such as $\mu^+ \rightarrow e^+\gamma$ and $\mu^+ \rightarrow e^+e^+e^-$ decays.

The energy distribution of muon Decay In Orbit (DIO) falls steeply above m_μ/2, but the DIO spectrum has a small tail extending to the conversion energy, Fig.2.1. Energy distributions for DIO electrons have been calculated for a number of muonic atoms [22,23] and the energy resolutions of the order of few percent are sufficient to keep this background low.

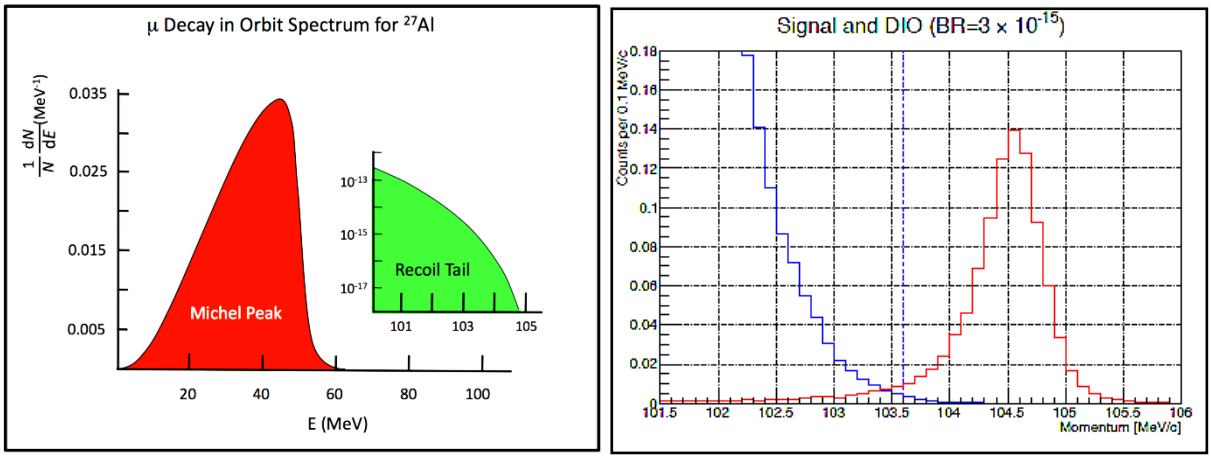

Fig. 2.1. Spectrum of electrons from muon decay in orbit. A tail of the distribution extends to the μ-e conversion energy.

Apart from decay in orbit, which is the main source of background, there are other potential sources of background:

i) background resulting from muon capture in atom:
   radiative muon capture;
   muon capture with emission of neutrons or charged particles;
ii) beam-related backgrounds:
   radiative pion capture;
   muon decay in flight;
   pion decay in flight;
   electrons in the beam;
   background induced by neutrons and antiprotons;
iii) cosmic rays background.

All the above sources have been thoroughly estimated and found acceptably small.

2.4. Mu2e experiment at FNAL.

The Mu2e experiment [24] at the Fermi National Laboratory (FNAL) has the same goal of search for $\mu^- \rightarrow e^-$ conversion. The muon beam line and detector for the Mu2e experiment are similar to those of the MECO experiment at BNL. Their planned single-event sensitivity (SES) is 3 x 10^{-17} (what is equivalent to the goal of COMET) with 3 years of 2 x 10^7 second running per year, although COMET needs only less than 1 year.

While the main structure of the experimental setup is similar to COMET, there are some differences in the beamline shape (S-shape in Mu2e vs C-shape in COMET), calorimeter structure etc. The Mu2e experiment would strongly compete with the COMET experiment.

3. Method of observation

A schematic drawing of the experimental setup is shown in Fig. 3.1. An 8 GeV proton beam from the J-PARC Main Ring (MR) collides with a target to produce pions. The pions emitted backward are captured with high efficiency using a 5 *T* superconducting solenoid magnet surrounding the pion-production target. The muons, which are produced by pion decays, are captured and transported through subsequent solenoids and are brought to a muon-stopping target in the detector solenoid. The muon beam line is composed of a combination of straight and curved superconducting solenoids. The curved solenoids are used to select the charge and momentum of muons in the beam line and have a compensating dipole magnetic field overlaid. The expected muon beam intensity is enormous, about 10^{11} μ^-/sec, which would be the highest in the world. The proposed method to create a very intensive muon beam has been proved at the MuSIC facility in Osaka where $3x10^8$ s^{-1} muon beam was obtained [25] with only 400 W proton beam power.

The experimental setup consists of the *muon beam line* and the *detector section*. The muon beam line is composed of the *pion capture solenoids* with high magnetic field, and the *muon transport with curved and straight solenoids*. The detector section is composed of the *muon stopping target*, the *electron transport* for $\mu^- \rightarrow e^-$ conversion signals, and *the detector*.

The C-shape design of the muon transport and the electron transport is an essential advantage of the COMET experiment. Muon transport section selects muons of low momenta in order to be stopped efficiently in the muon stopping target . Electron transport section, vice versa, is tuned to select high energy electrons arising from μ-e conversion in the target and to eliminate low-energy electrons that could make background hits to the detector.

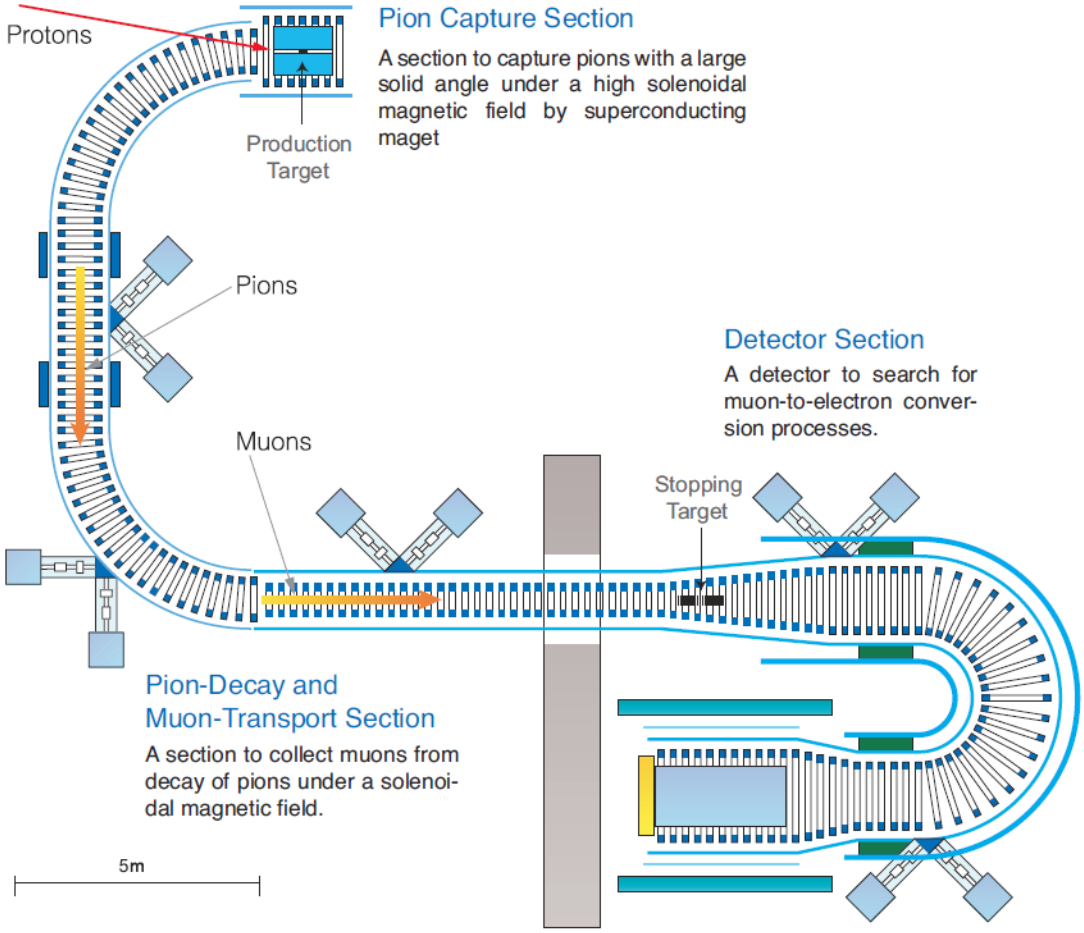

Fig.3.1. The COMET experiment schematic layout. Magnetic fields of the superconducting solenoids range from 5 to 1 Tesla.

3.1. Proton beam and pion production

The number of pions (and therefore their daughter muons) produced by a proton beam is proportional to the proton beam power, which is given by the product of the beam energy and beam current. The proton beam power of the current design is 8 GeV × 7 μA (4.4×10^{13} protons/second), which will provide enough muons for COMET to achieve its physics goal within about one year of running (8.5×10^{20} protons to produce 2×10^{18} muons). Note that the J-PARC proton beam will be used not at full energy and power.

The proton beam needs to be pulsed with a time separation of the order of 1 μs, which corresponds to the lifetime of a muon in a muonic atom (0.864 μs in Al). Short beam buckets, compared with this lifetime, would allow removal of prompt beam background events when performing measurements in a delayed time window, as shown in Figure 3.2. The required separation between the proton beam pulses will be realized by filling every third bucket, which gives a total of three out of nine. The scheme is illustrated in Fig. 3.3.

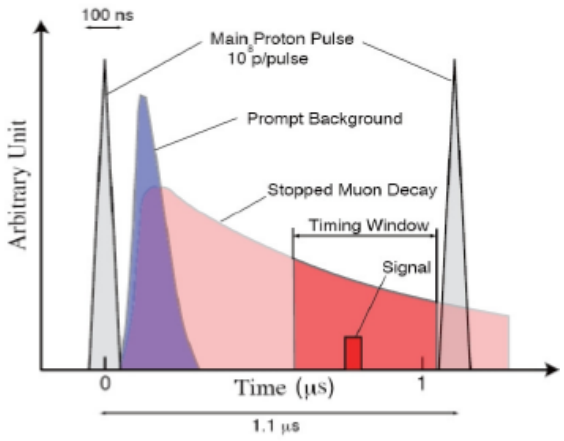

Fig. 3.2. Time structure of the proton beam and timing window for measurements.

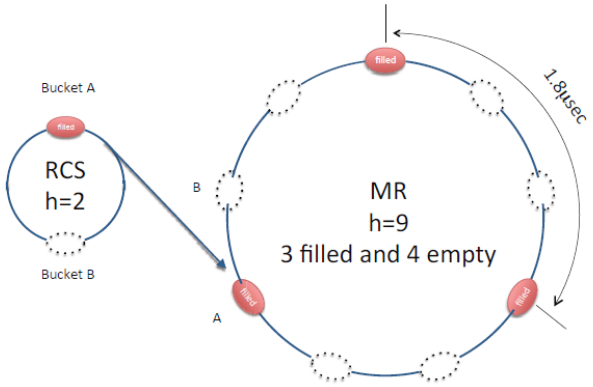

Fig. 3.3. The proposed bunch configuration for COMET.

It is very important to reduce the number of residual protons between the pulses as these will produce beam related background in the signal timing window. For COMET to achieve its expected sensitivity the relative number of residual protons between the pulses ("*proton extinction factor*") need to be 10^{-9} or less of the number of protons in the pulse. The dedicated measurement of the proton extinction factor at the J-PARC accelerator ring has achieved even the better value, of the order of 10^{-11}.

The COMET experiment uses negatively charged low-energy muons, which can be stopped in a muon-stopping target. The low-energy muons are mostly produced by in-flight decay of pions of low energy. Therefore, the production of low energy pions is of major interest. At the same time, high-energy pions, which could potentially cause background events, should be eliminated as much as possible.

The π^- production yields by protons incident on graphite and tungsten are presented in Fig.3.4. It is seen that high-energy pions are suppressed in the backward direction. For this reason, it has been decided to collect pions emitted backward with respect to the proton beam direction.

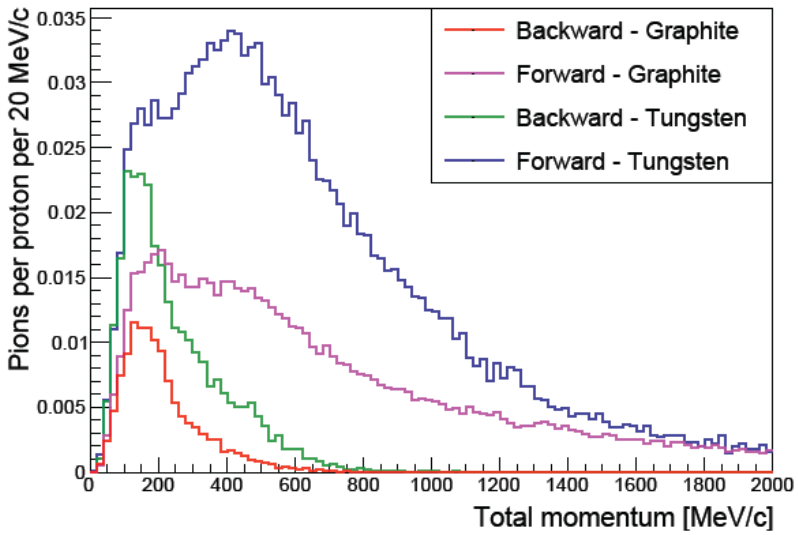

Fig. 3.4. Pion production in graphite and tungsten targets: total momentum distributions for forward and backward π^-.

3.2. Muon transport section

Muons and pions are transported to the muon-stopping target through the muon beam line. The requirements for the muon transport section are:

- the muon transport should be long enough for pions to decay into muons. For instance, for about 20 meters, the pion survival rate for pions with the reference momentum is about 2×10^{-3} ,
- the muon transport should have a high transport efficiency for muons with a momentum of low momentum around 40 MeV/*c*,
- at the same time the muon transport should eliminate muons of high momenta (p_μ> 75 MeV/*c*) to avoid backgrounds from muon decays in flight since their decays in flight would produce spurious signals of ~105 MeV electrons.

The design of the muon transport section utilizes two curved solenoids with a bending angle of 90º in the same bending direction (see Fig. 3.1), and a straight solenoid between the two. The curved solenoid causes the centers of the helical motion of charged particles to drift perpendicular to the plane in which their paths are curved. To keep the center of the trajectory of the low energy muons, the compensating dipole fields are applied.

3.3. Detector section

Detector section (Fig. 3.5) includes muon-stopping target, electron transport section and the detector itself.

The muon-stopping target is placed in the center of the muon-target solenoid. The muon-stopping target is designed to maximize the muon-stopping efficiency and the acceptance for the $\mu^- N \rightarrow e^- N$ conversion electrons and to minimize the energy loss of the conversion electrons in order to minimize the momentum spread of the electrons.
The muon-stopping target configuration is shown in Table 3.1.

Table 3.1. Configuration of the COMET muon-stopping target

Item	Specification
Material	Aluminum
Shape	flat disk
Disk radius	100 *mm*
Disk thickness	200 μm
Number of disks	17
Disk spacing	50 *mm*

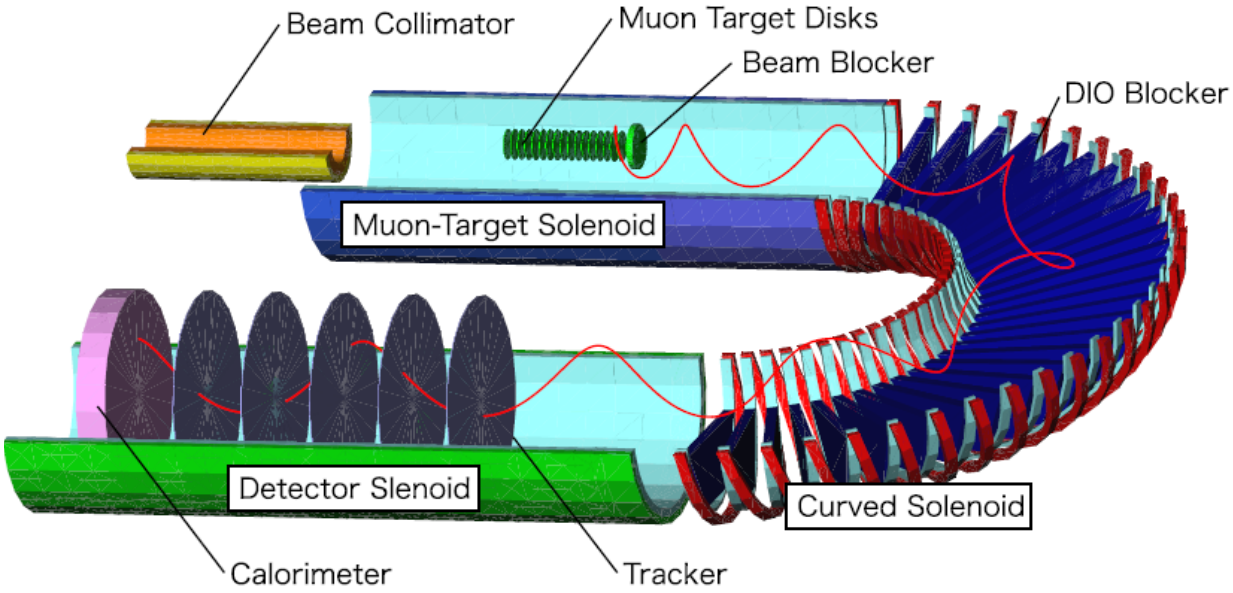

Fig. 3.5. Detector section of the COMET consisting of the muon-target section, the electron-transport section and the particle detector section. A typical conversion signal track is shown in red.

A beam collimator is placed upstream of the stopping target, and a muon beam stop is placed downstream of the last target disk.

The requirements of the electron transport in the COMET electron spectrometer are:

- to remove charged-particle backgrounds of low momenta so as to reduce single counting rates of the detectors, and
- to maximize the transmission of $\mu^- \rightarrow e^-$ conversion signals.

The electron transport consists of curved superconducting solenoids with collimators inside the solenoid. Like in the muon transport section, a charged particle in a uniform solenoidal field moves along a helical trajectory. Tracks with desired momentum (105 MeV/*c*) stay nearly in a horizontal plane using a drift-compensating dipole field. On the other hand, tracks with wrong momenta drift to upward and are absorbed by a collimator.
The electron transport ends with a detector solenoid which contains the detector of the conversion electrons.

4. Detector

The main purpose of the COMET detector is to distinguish electrons from other particles and to measure their energies, momenta, and timing. The detector consists of an electron tracker with straw-tube gas chambers for measuring momenta of electrons and an electromagnetic calorimeter for measuring their energies. The detector is placed under a uniform solenoidal magnetic field of 1*T*. Furthermore, to reduce multiple scattering in momentum measurements, the entire system is placed under vacuum.

4.1. Tracking detector

Since the momentum of the electrons from $\mu^- \rightarrow e^-$ conversion is as low as 105 MeV/*c*, the intrinsic momentum resolution is dominated by multiple scattering of electrons in the tracker material. Therefore, reduction of a total mass of the tracking detector and placing it in a vacuum environment are of great importance. For these requirements, a straw-tube gas wire chamber technology has been selected for the tracker. The straw tracker is based [26] on that being built for the NA62 experiment at CERN.

The overall structure of the straw tracker is shown in Fig. 4.1. It consists of a set of 5 stations of straw-tube planes, and placed so that the axial direction of the straws is transverse to the axis of the solenoid. Each of the 5 stations contains a set of 4 straw tube arrays, two for *x*- and two for *y*-coordinates.

Both timing and pulse height information are recorded from one end of each hit wire. Pulse height is used to discriminate between electron and low-energy, heavily ionizing tracks (e.g. protons) which can occur through the atomic muon absorption on nuclei.

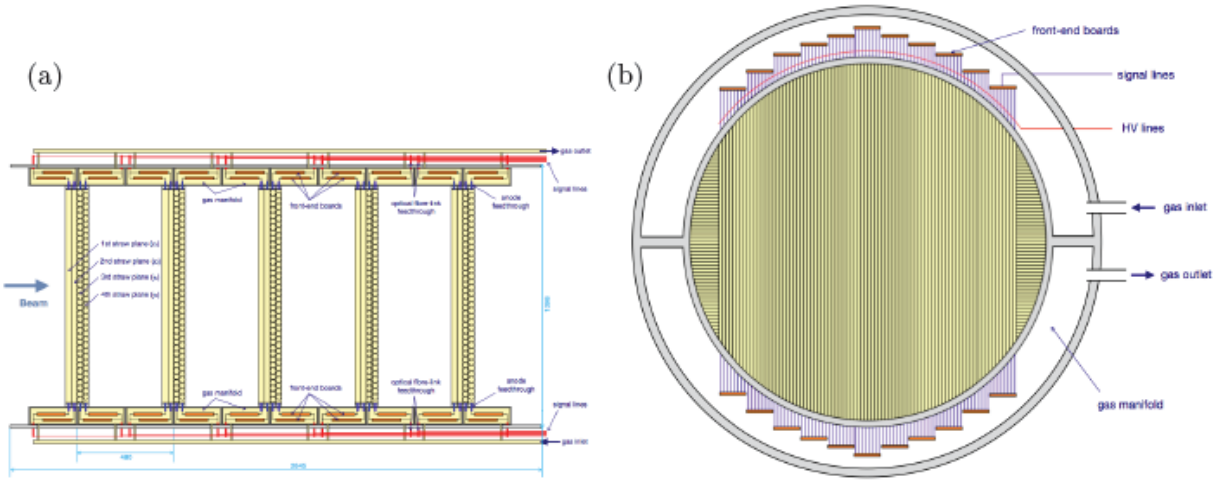

Fig. 4.1. (a) Side view of the straw tracker, and (b) cross-sectional view of a plane.

The straws will have a diameter 5 *mm* or 9.75 *mm* (the latter at the Phase-I of the experiment as explained below). A default gas mixture is 50/50 Ar/C_2H_6.

The required momentum resolution is 150 keV/c (RMS), space resolution is 150 μm.

4.2. Electromagnetic calorimeter

The electromagnetic calorimeter (ECAL) system (Fig.4.2.) consists of segmented scintillating crystals. It is placed downstream of the straw chamber detector and serves the following purposes:

- to measure the energy of electrons *(E)*, where good energy resolution is necessary;
- to provide the *E/p* ratio for the electron identification. Redundant measurements of energy and momentum of electrons are of critical importance to identify the μ−e conversion signal events from backgrounds;
- to provide a timing signal, i.e. a trigger, with respect to which the electron events are referenced;
- to provide additional position information on the electron track trajectory correlating the measured energy with the track and eliminating false tracking.

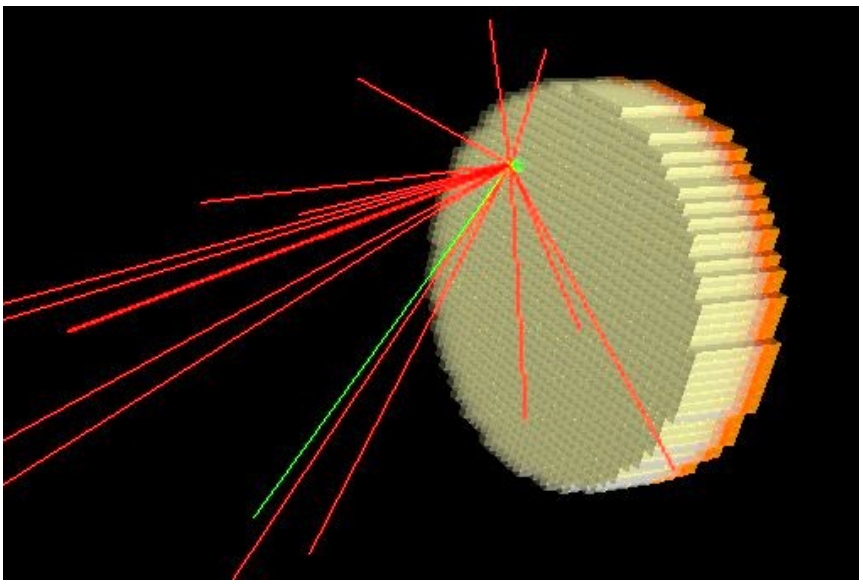

Fig.4.2.The electromagnetic calorimeter.

Energy resolutions of the calorimeter has been studied using Geant4 with Optical Photon Processes. The resolution depends on crystal, light guide, photon detector, and their geometrical configuration. This selection would be a cost effective case for the photon detector, since the ratio of active area of the photon detector to the cross section of the crystal is set to 0.09.

The ECAL is required to have energy resolution better than 5% at 100 MeV and a cluster position resolution better than 1 cm. With sufficient crystal granularity the shower topology can also be used to discriminate electrons from neutrons and low energy photons. The crystals need to have a good light yield, and a fast response- and decay-time to reduce pileup.

From two the best crystal candidates with large light yield and small decay constant, which are GSO(Ce) and LYSO(Ce), the latter has been selected after the beam tests of the prototype. The calorimeter will consist of the LYSO crystals of 2x2 cm^2 cross section and 12 *cm* length (about 10.6 radiation length). To covers the full cross-section of the detector region, about 2000 crystals is needed.

Because operation of the calorimeter is in a 1 T field, scintillation light will be read out with the Avalanche Photo Diodes (APDs), and the options of 5x5 and 10x10 mm^2 sensitive area are under test.

4.3. Cosmic ray veto

Cosmic ray induced electrons (or other particles misidentified as electrons) may cause background events. Therefore, passive and active shielding against cosmic rays will be arranged covering the entirety of the detector. Figure 4.3 shows a preliminary layout of the cosmic ray shield.

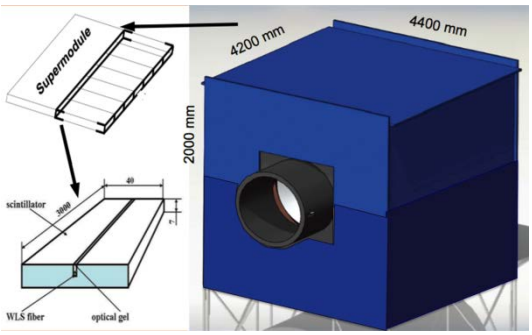

Figure 4.3: Schematic view of cosmic-ray active shield covering the whole detector.

The passive shielding will be a combination of steel and concrete walls. The active shielding placed inside the passive shielding, will consist of four layers of scintillator strips with a WLS fiber readout. With 99% efficiency of each scintillator layer, the cosmic ray system inefficiency will be 10^{-4}.

5. Two-stage realization of the COMET experiment.

Taking into account the risks of an ambitious goal to increase 10000 times the sensitivity of measurements, it is necessary to study experimentally all expected background processes and possible obstacles. With this aim, the project is split into two phases. The final declared experiment sensitivity will be reached at Phase-II. At Phase-I the goals will be two-fold: i) to estimate the experimental conditions and measure the backgrounds, and ii) to search for μ-e conversion with an intermediate sensitivity.

5.1. COMET Phase-I

The main differences of Phase-I [27] compared to Phase-II are the following:

- pion-decay and muon-transport section ends after the first 90^0 bend, Fig. 5.1;
- the proton beam power will be reduced to 3.2 kW (compared to 56 kW at Phase-II);
- two detector configurations will be used (as explained below);

- a carbon pion production target (instead of tungsten) will be used which does not require cooling at this reduced beam power.

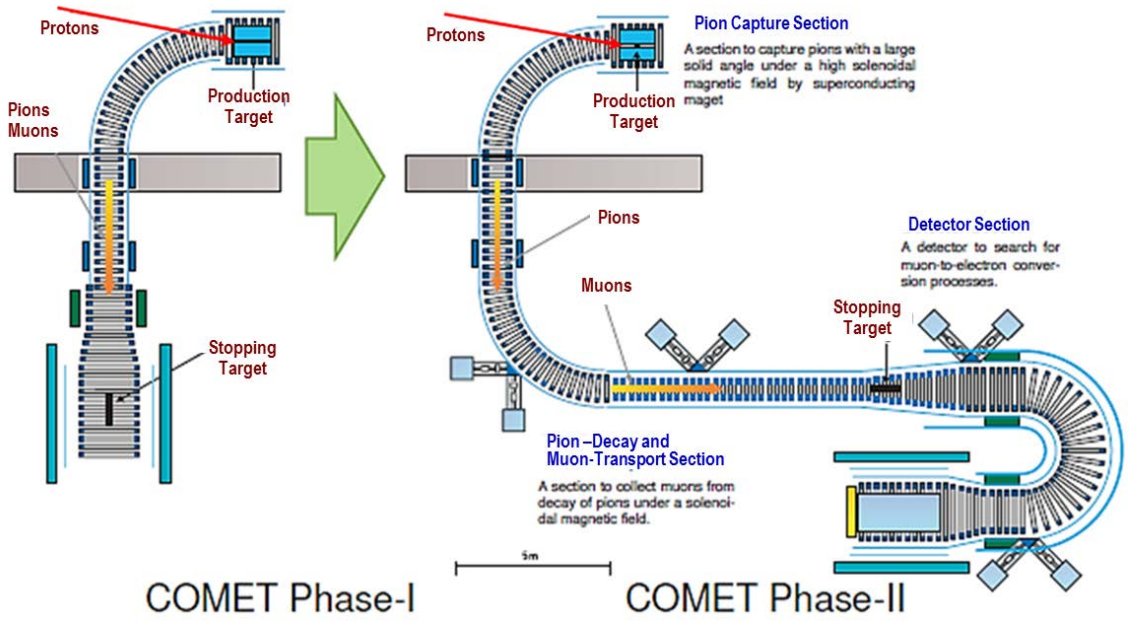

Fig. 5.1. Beam line configurations at Phase-I and Phase-II.

Note that in Phase-I there will be no curved solenoid system between the muon stopping target and the detector, and therefore beam particles which do not stop in the muon stopping target would hit the downstream detectors causing a heavy background load.

The main goals of the COMET Phase-I are:
1) the direct measurement of the proton beam extinction and other potential background sources for the full COMET experiment, using the actual COMET beam line, and
2) carrying out a search for $\mu^- \rightarrow e^-$ conversion with a single-event sensitivity of 3.0×10^{-15} which is 200 times better than the current world best SINDRUM-II limit.

The detector configurations for these two goals will be different, once they are optimized for their best performance. For the μ-e conversion search at COMET Phase-I a cylindrical detector , which will be placed at a 90 degree from the muon stopping target with respect to a muon beam-line, is the best choice as it does not “see” forward beam particles. For the beam background studies another configuration consisting of the straw tracker and electron calorimeter is a good option. It is expected that the straw tracker and calorimeter constructed for Phase-I can be directly used at COMET Phase-II, as well.

5.1.1. Detector for background measurements

Exactly the same detector technology as for the main COMET detector will be employed. Figure 5.2 shows schematic view of the setup for background measurement. The setup includes 5 super-layers of straw chamber tracker and a crystal calorimeter composed of LYSO crystals. At Phase-I the calorimeter will use not a full set of crystals but about a quarter of it, ~500 pieces. The requirements to straw tracker at Phase-I are loosened: the tubes will be of 9.8 mm diameter and 20 μ wall thickness (instead of 5 mm and 12 μ, respectively, at Phase-II). It is planned and quite feasible that the tracker and the calorimeter prepared for Phase-I will be later used at Phase-II with only minor modifications.

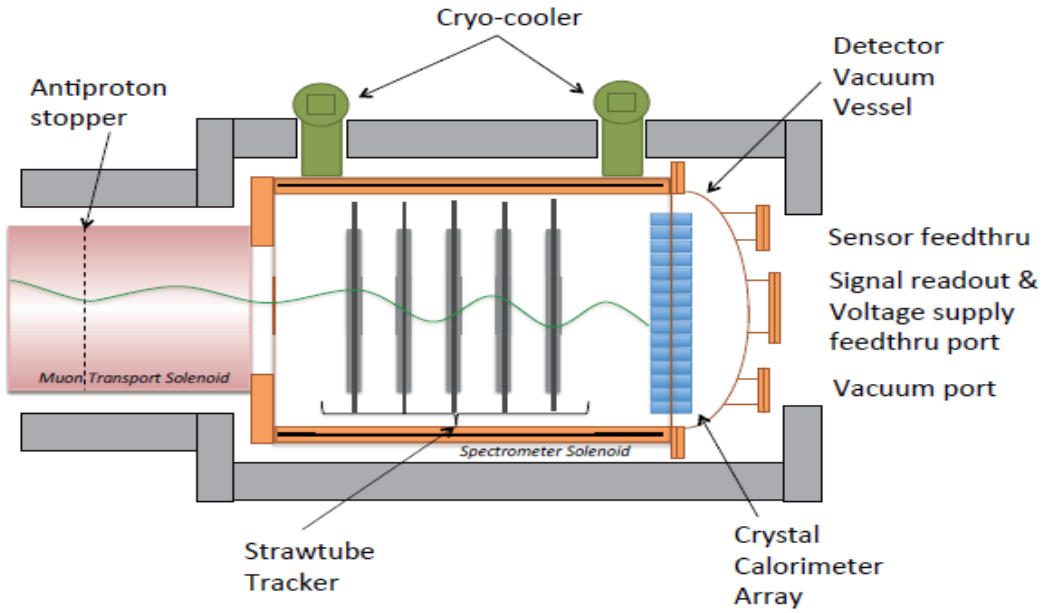

Fig.5.2. Setup for the background measurement in COMET Phase-I.

Use of this detector configuration for μ-e conversion search at Phase-I is problematic due to absence (at this stage) of the electron transport system with curved solenoids, and hence expected high rates in these detectors. Therefore, their use for $\mu^- \rightarrow e^-$ conversion search at Phase-I is possible only at low beam intensities.

5.1.2. Cylindrical Detector for the $\mu^- \rightarrow e^-$ conversion search

More favorable detector option for the $\mu^- \rightarrow e^-$ conversion search at Phase-I is using of a ***cylindrical detector***. Figure 4.3 shows schematic view of the detector setup.

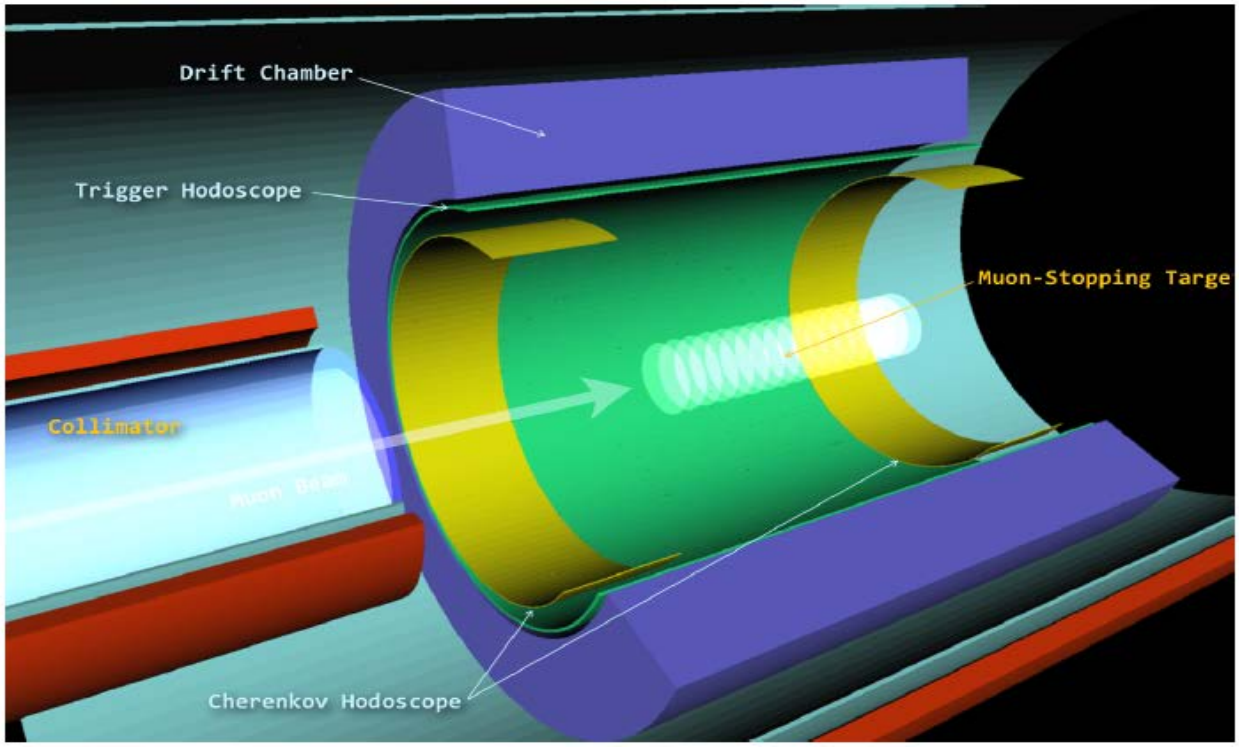

Fig.4.3. Schematic view of the cylindrical detector for $\mu^- \rightarrow e^-$ conversion search.

The setup is based on a Cylindrical Drift Chamber (CDC) which surrounds a muon stopping target and trigger counter placed in front of the tracker chamber. The detector structure is similar to the SINDRUM-II detector [28, 29]. At COMET Phase-I a search for $\mu^- \rightarrow e^-$ conversion in aluminum will be carried out with a single-event sensitivity of 3.0×10^{-15}.

In addition to the $\mu^- \rightarrow e^-$ conversion search, there are special features of the COMET Phase- I cylindrical detector allowing for further possibilities:

• With a cylindrical configuration one can detect both positive and negative particles. This allows for a search for the lepton-number-violating process $\mu^- + N \rightarrow e^+ + N'$ ($\mu^- \rightarrow e^+$ conversion) concurrently with the $\mu^- \rightarrow e^-$ conversion search.

• This detector can have a large geometrical coverage, and thereby a coincidence measurement with a large solid angle is achievable. Therefore, it is possible to search for the previously-unmeasured process, $\mu^- + e^- \rightarrow e^- + e^-$ conversion in a muonic atom.

5.2. COMET Phase-II

This final stage includes creation of a full beam line, use of higher beam intensity, and change of the detector configuration. The 8 GeV proton beam power will increase from 3.2 *kW* at Phase-I to 56 *kW* at Phase-II. The main detectors for the $\mu^- - e^-$ conversion search will be straw tracker and ECAL instead of CDC. These modifications, together with experience gained during Phase-I, will make possible to carry out a search for $\mu^- - e^-$ conversion at the single-event sensitivity of $3 \cdot 10^{-17}$.

In Table 5.1 comparison of the Phase-I and Phase-II parameters is given.

Table 5.1. COMET Phase-I and Phase-II parameters.

	Phase-I	Phase-II
Beam power	3.2 kW (8 GeV)	56 kW (8 GeV)
Exposition time	150 days	1 year
Proton beam target material	graphite	tungsten
#protons on target	2.37×10^{19}	8.5×10^{20}
#muon stops	1.3×10^{16}	2.0×10^{18}
Muon flux	5.8×10^{9}	1.0×10^{11}
Background events	0.02	0.3
Single event sensitivity	3.1×10^{-15}	2.6×10^{-17}
Upper limit (90% CL)	7.2×10^{-15}	6.0×10^{-17}
Planned start of measurements	2018-2019	2021

6. JINR contribution to the COMET experiment

The main contribution of JINR to COMET consists of participation in the production of two main detector systems – the electromagnetic calorimeter and the straw tracker, and includes variety of works on a simulation.

Below we present what has been done and our plans for the following period.

6.1. Electromagnetic calorimeter.

From the beginning of the R&D works related to the COMET experiment the JINR group has proposed two types of scintillating crystals, GSO and LYSO, which became considered in the collaboration as the real candidates. In order to evaluate their adequacy for COMET, a lot of laboratory studies have been done in DLNP JINR. Some optical properties (energy resolution, light output, non-uniformity of light yield) of LYSO and GSO crystals were studied [1]. In DLNP a dedicated high precision test bench for measuring the crystal parameters has been arranged (Fig.6.1). The test bench includes a mechanical arrangement for remote-controlled movement of the crystal, photomultipliers for light readout, plastic veto-counters, corresponding electronics and software. All the work on the data acquisition, the movement of RA-source to the desired position along the surface of the crystal with the required accuracy was automated. The correlation algorithm for selection in the trigger system was used to reduce the impact of intrinsic radioactive radiation on the energy resolution of LYSO crystal. These studies have shown the advantages of the LYSO type which, however, is more expensive compared to GSO. Therefore, the final decision about selection of the LYSO crystals has been done after the test of the calorimeter prototypes (both GSO and LYSO) with an electron beam in Tohoku University and takes into account the cost/performance ratio.

The crystals used in the LYSO prototype (50 pieces) have been thoroughly investigated in DLNP JINR [2] first, including light yield, light absorption, homogeneity etc.

Later on the JINR physicists participated in assembling of the prototype, beam measurements and fulfilled independent analysis of the beam test results. Following these investigations, the collaboration has selected the LYSO crystal as one to be used in the calorimeter.

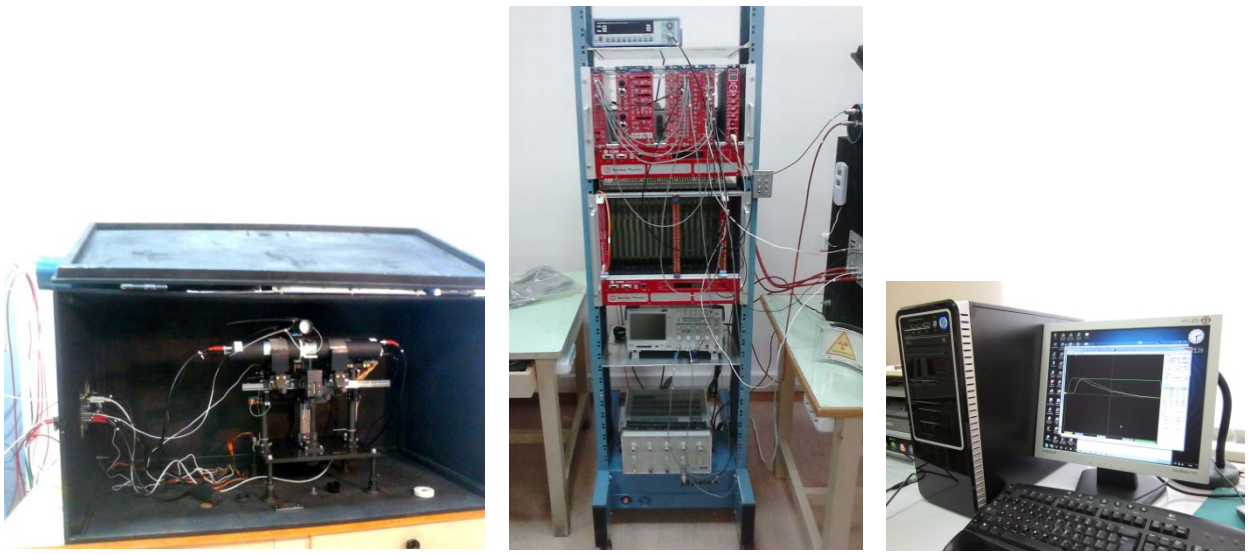

Fig.6.1. Test bench to measure the crystal quality.

We plan plan to test all crystals for the calorimeter with this test bench in JINR.

JINR takes full responsibility for testing of the LYSO crystals to be used in COMET Phase-I and Phase-II. We will continue the study of the crystal properties, light readout options, different wrapping materials etc. The preliminary results are given on the Fig.6.2.

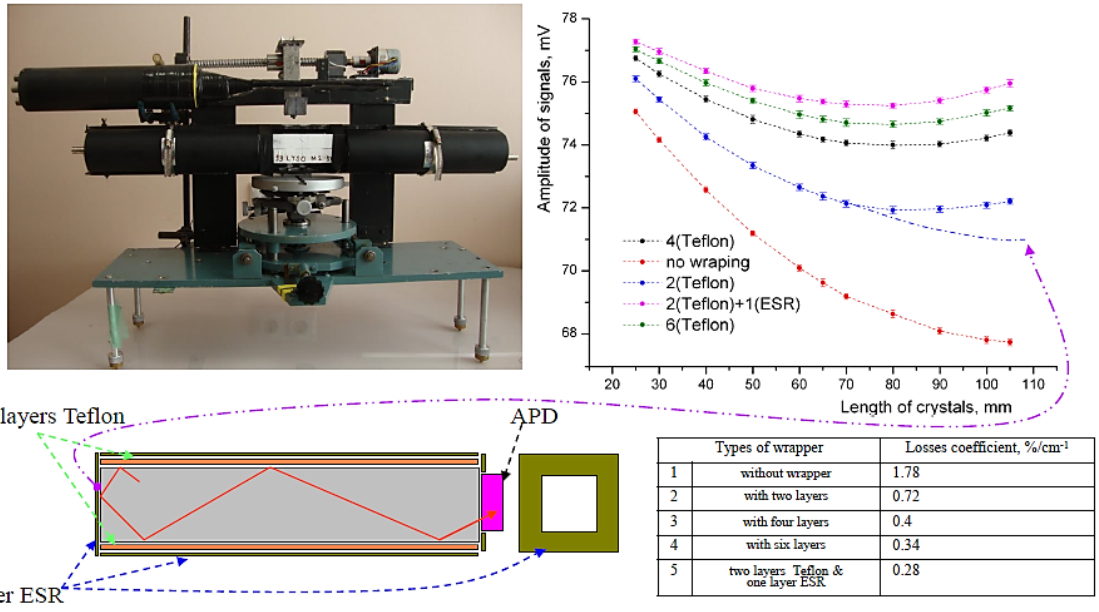

	Types of wrapper	Losses coefficient, %/cm^{-1}
1	without wrapper	1.78
2	with two layers	0.72
3	with four layers	0.4
4	with six layers	0.34
5	two layers Teflon & one layer ESR	0.28

Fig.6.2. Dependence of the signal attenuation along the crystal on reflecting material.

It is necessary to note that the JINR participates in the engineering design of the calorimeter as well. Finally, the JINR physicists will take part in an assembling, calibration and tests of the calorimeter.

6.2. Straw tracker

The JINR group is a single one in the COMET collaboration which is capable to produce thin-wall straw tubes. Therefore, we are fully responsible for manufacturing of all straw tubes.

As the method for the straw tube production, an ultrasonic welding method, developed in JINR by the VBLHEP group participating in experiment NA62 at CERN, has been used. For NA62 they have produced few thousands of the straw tubes of 9.5 mm diameter and 36 μm wall thickness. Note that this thickness is too large for COMET.

The Laboratory of High Energy Physics has kindly allowed us to use their facility for production of straw tubes for COMET Phase-I, and VBLHEP physicists provided us with necessary training. After that the COMET participants were able to work without assistance. They have developed the technology of production thinner tubes, of 20 μm wall thickness aluminized Mylar (70 nm Al layer), what is more suitable for the Phase-I.

Different procedures of the tube tests on pressure, gas leakage and elongation have been also updated in accordance with the COMET requirements and new test standards have been established.

As a result, a full set of straw tubes for Phase-I, more than 2500 tubes of 120 and 160 cm length, 9.8 mm diameter and 20 μm wall thickness, has been produced and delivered to Japan (Fig.6.3).

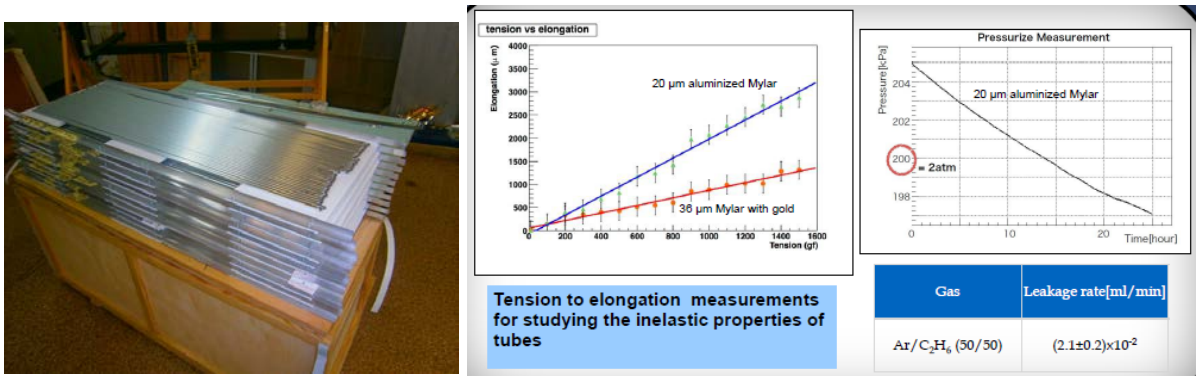

Fig.6.3. Left: straw tubes prepared for shipping. Right: results of the leakage and elongation tests.

The next step to this direction is preparation and carrying out of R&D works of straw tubes for the COMET Phase-II. At Phase-II we need the tubes of 5 mm diameter and 12 μ wall thickness. For this purpose within the framework of R&D works we are planning to arranging a new straw line in our Laboratory of Nuclear Problems. The method of manufacturing will be the same, the ultrasonic welding, but the extensive R&D works need to be done in order to deal with such a delicate material. The technology of the production process and the procedures of testing have to be updated for new conditions. A part of equipment is already available, and the rooms for straw tubes R&D works are in preparation.

The JINR physicists will be involved in assembling and tests of the full scale straw tracker, first for Phase-I and then R&D works for straw tracker for Phase-II of COMET.

Another JINR activity related to the straw tracker is engineering design of the detector including design of the supermodules, optimization of readout electronics boards arrangement inside the

gas manifold and integration of the five supermodules in the vacuum volume (Fig.6.4)

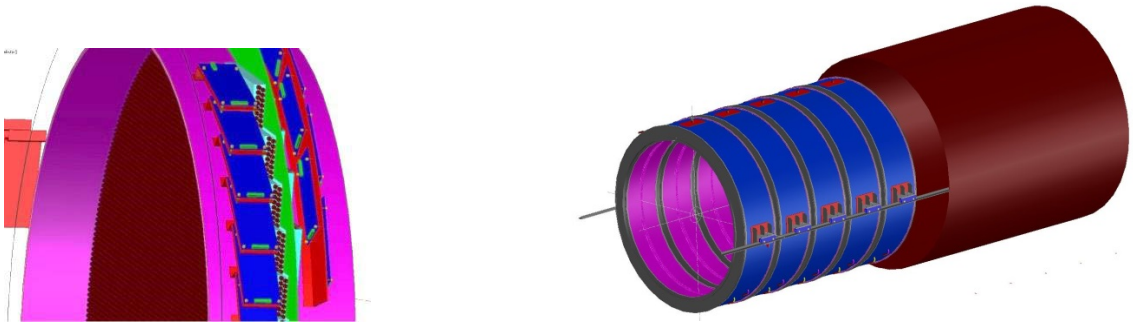

Fig.6.4. Examples of the design developments. Left: two options for attachment of the electronics. Right: five straw modules fixed on rails to be moved into the solenoid.

6.3. Simulation and Data Analysis

Development of the straw tracker and calorimeter systems required a lot of simulation work. The corresponding results are presented in the Technical Design Report for Phase-I of COMET [27]. In particular, the values of efficiency and space resolution in different conditions: for the tubes of different diameters, wall thicknesses and gaps between the tubes, for the straw tracker have been established. Similarly, the calorimeter simulation has been done for two types of crystals, GSO and LYSO using the real optical parameters. Among others, simulation of light outputs and light collection with different reflecting materials also has been performed. Simulated energy resolution was found to be better for the LYSO type what has been confirmed later experimentally.

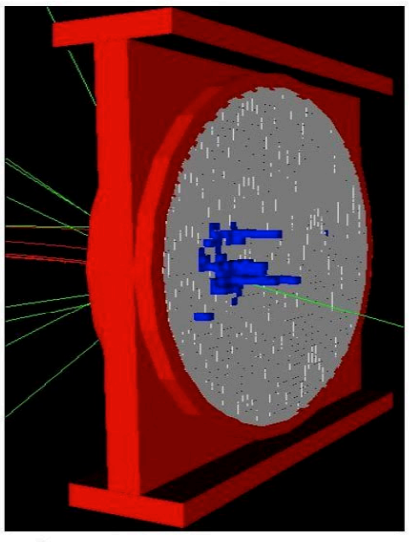

The Geant4 simulation of the optimal structure of the segmented calorimeter for the COMET experiment was made (Fig. 6.5). The simulation of the electromagnetic calorimeter was included in the framework ICEDUST (Integrated Comet Experimental Data User Software Toolkit), which is adopted framework for any COMET software activity .

A dedicated simulation has been done with the aim to optimize the operation of the J-PARC Main Ring in order to achieve very low extinction factor, below 10^{-9}, what is the must for COMET.

The data from the calorimeter prototype beam test has been analyzed independently in Japan, based on the similar analysis. Both analyses have led to the conclusion about a better performance of the LYSO crystals.

Fig.6.5.The calorimeter (GEANT4 simulation).

In the future, we are planning to enlarge our scope of works on simulation and analysis in order to be ready for a physic analysis for the COMET data from J-PARC.

7. Financing

An overwhelming part of COMET expenses, in particular its facility, bears the KEK side. It fully finances the constructions of the proton beam line, the muon and electron transport system and the experimental zone. Production of the detectors will also be mainly financed by the the KEK, Japanese universities and other collaborating participants. Expenses of JINR come from R&D program to study a new type of straw tubes, purchasing of necessary equipment and materials including a part of crystals. Apart from the resources of the JINR theme, we are expecting the support from the Grant of Plenipotentiary of Georgia and from the Program of the JINR-Belarus Cooperation.

8. Conclusion

The experiment COMET at J-PARC is focused at a search for coherent neutrino-less conversion $\mu^- + Al \rightarrow e^- + Al$ in a muonic atom of aluminum at the level of a single-event sensitivity (SES) $3 \cdot 10^{-17}$, corresponding to a 90% confidence level $< 10^{-16}$.

The two-fold goal of Phase-I of COMET includes i) studies of experimental beam conditions and different sources of background, and ii) a search for the $\mu^- \rightarrow e^-$ conversion with intermediate sensitivity of SES $\approx 3 \cdot 10^{-15}$, which is 200 times better than the current limit.

The role of JINR in the COMET experiment is quite visible and recognized by the COMET Collaboration.

Concluding, we apply for the extension of the current JINR project “Search for coherent neutrino-less μ - e conversion at J-PARC (project C)” for 2017-2019. This period well fits to the beginning of physics measurement at Phase-I, which is planned for 2018-2019, and carrying out R&D program to study a new type of straw tubes for Phase-II, which is scheduled to start in 2021.

References

[1] COMET, Y.G. Cui et al., CDR, KEK-2009-10

[2] Super-Kamiokande Collaboration, Fukuda Y. et al., Phys. Rev. Lett. **81** (1998) 1562-1567. http://link.aps.org/doi/10/1103/Phys.RevLett.81.1562.

[3] Super-Kamiokande Collaboration, Fukuda Y. et al., Phys. Rev. Lett. **86** (2001), 5656-5660. http://link.aps.org/doi/10/1103/Phys.RevLett.86.5656.

[4] Cheng T.P. and Li L.F., Phys. Rev. **D16** (1977) 1425-1443. http:/link.aps.org/doi/10.1103/Phys.Rev.D.16.1425.

[5] Lee B.W. and Shrock R.E, Phys. Rev. **D16** (1977) 1444-1473. http:/link.aps.org/doi/10.1103/Phys.Rev.D.16.1444.

[6] Petcov S., Sov.J.Nucl.Phys. **25** (1977) 340.

[7] Marciano W. and Sanda A., Phys. Lett. B. **67**, no.3, (1977) 303-305.

[8] Yanagida T, in Proceedings of the Workshop on Unified Theory and Baryon Number of the Universe, edited by Sawada and Sugamoto, Report KEK-79-18 (1979); Gell-Mann M, Ramond P, and Slansky R, in Supergravity, edited by D.Z. Freedman and P. van Nieuwenhuizen (North-Holland, Amsterdam, 1979).

[9] Hisano J, Moroi T, Tobe T, Yamaguchi M, and Yanagida T 1995 Phys. Lett. B **357**, 576.

[10] Hisano J and Nomura D 1999 Phys. Rev. **D59** 116005.

[11] Sato J amd Tobe T, 2001 Phys. Rev. **D64** 113016.

[12] Cirigliano V, Kitano R, Okada Y, and Tuzon P, arXiv:0904.0957v1 [hep-ph].

[13] Arkani-Hamed N , Cohen A. G., and Georgi H , 2001 Phys.Rev.Lett. **86** 4757.

[14] Arkani-Hamed N, Cohen A.G. , Katz E, and Nelson A E. 2002 JHEP **0207** 034.

[15] Choudhury S. R., Cornell A. S., Deandrea A, Gaur N, and Goyal A, 2007 Phys. Rev **D75** 055011.

[16] Blanke M, Buras A. J., Duling B, Poschenrieder A, Tarantino C 2007 JHEP **0705** 013.

[17] Aguila F, Illana J.I. , Jenkins M. D., 2009 JHEP **0901** 080.

[18] Randall L, and Sundrum R, 1999 Phys. Rev. Lett **83** 3370.

[19] Appelquist T , Cheng H. -C , and Dobrescu B, 2001 Phys. Rev. **D64** 035002.

[20] Kuno Y. and Okada Y., Rev. of Mod. Phys. **73** (2001) 151.

[21] Bertl W. et al. (The SINDRUM II Collaboration); Eur. Phys. J. C, **47** (2006) 337-346.

[22] Shanker O.U., et al., Phys.Rev. **D25** (1982) 1847.

[23] Watanabe R., et al., Prog.Theor.Phys. **78** (1987) 114-122.

[24] A research proposal to Fermilab: "Proposal to Search for $\mu^- N \rightarrow e^- N$ with a Single Event Sensitivity Below 10^{-16} (Mu2e experiment)", 2008. http://mu2e-docdb.fnal.gov/cgi-bin/RetrieveFile?docid=388;filename=proposal_v34.pdf;version=1.

[25] S.Cook et al. Journal of Physics: Conf. Series **408** (2013) 012079.

[26] Azorskiy et al. "Design and Test Results of NA62 Straw Detector First Prototype", Preprint JINR P13-2013-50, Dubna, 2013.

[27] COMET Phase-I TDR, COMET Collaboration, 2014. http://comet.kek.jp/Documents_files/IPNS-Review-2014.pdf

[28] Dohmen C. et al. (SINDRUM II Collaboration), Phys. Lett. B, **317** (1993) 631.

[29] Honecker W. et al. (SINDRUM II Collaboration) Phys. Rev. Lett., **76** (1996) 200.

Papers of the project authors related to the COMET experiment:

1. V.Kalinnikov, E.Velicheva. Investigation of LYSO and GSO crystals and simulation of the calorimeter for COMET experiment. Physics of Particles and Nuclei, Letters, **11**, №3, 259 (2014).

2. В.Калинников, Е.Величева. Исследование параметров и разработка алгоритма пространственной реконструкции для калориметра COMET эксперимента. Физика сцинтилляторов. Материалы, методы, аппаратура, с.186 (2014).

3. В. Калинников, Е. Величева, А. Лобко. Исследование длинных кристаллов GSO и LYSO для создания сегментированных электромагнитных калориметров. Физика сцинтилляторов. Материалы, методы, аппаратура, с.137 (2014).

4. V.Kalinnikov, E.Velicheva. Research of Long GSO and LYSO Crystals Used in the Calorimeter developed for the COMET Experiment. Functional Materials, **22**, №1, p.126 (2014).

5. V.Kalinnikov, E.Velicheva. Research of the ECAL calorimeter used in the COMET experiment. Functional Materials, **22**, №1, 116 (2014).
6. M. Eliashvili, A.Khvedelidzre, M.Nioradze, Z. Tsamalaidze, THE COMET EXPERIMENT AT J-PARC: A STEP TOWARDS SOLVING THE MUON ENIGMA, TSU Science, N6, (2014)

7. V.Kalinnikov, E.Velicheva. Simulation of Long GSO Crystals for the COMET Experiment. NONLINEAR PHENOMENA IN COMPLEX SYSTEMS, 18, №2, 215 (2015).

8. А.Д.Волков. Контроль натяжения трубок в строу детекторах. Успехи прикладной физики, 2,№4, 413 (2014).

9. A.D.Volkov. Wire tension monitor for proportional chambers of the ANKE spectrometer. NIM A 701, 80 (2013).

10. А.Д.Волков. Устройство для измерения натяжения трубки в строу детекторах. Патент 2539107 (2013).

11. N.Tsverava et al. Thin-wall straw tubes for experiment COMET (in preparation).

12. COMET Phase-I. Technical Design Report 2016 (prepared with participation of the JINR physicists).

13. H. Nishiguchi, P. Evtukhovitch, A. Moiseenko, Z. Tsamalaidze, N. Tsverava, A. Volkov, et al. Development of an extremely thin-wall straw tracker operational in vacuum- The COMET straw tracker system. Accepted NIM, 2016.

Schedule of works on the project

1.	Participation in assembling and tests of the straw detector for Phase-I	**2017-2018**
2.	R&D for production of the straw tubes of 12 μ wall thickness and 5 mm diameter for Phase-II:	**2017-2018**
3.	Test of the crystals in JINR to be used in the calorimeter:	**2017-2019**
4.	Participation in the calorimeter designing, assembling and tests:	**2017-2019**
5.	Participation in the beam tests of the detector components:	**2017-2019**
6.	Creation of the COMET computer farm in LIT-JINR	**2017**
7.	Complex detector system (tracker, calorimeter, etc.) simulation to define the acceptance, expected uncertainties, sources of systematics, reconstruction algorithm development, etc.	**2017-2019**
8.	Participation in assembling, installation and testing of the whole detector	**2017-2019**
9.	Participation in the engineering and physical run:	**2018-2019**
10.	Participation in the data acquisition and analysis:	**2019**

Estimation of costs and resources

Proposal for resources necessary for realization of the project ″Search for coherent neutrino-less μ -e conversion at J-PARC (COMET) ″, 2017-2019

Form №26

Units and systems of The setup, resources, Sources of financing			Cost of units (k$). Required resources	Laboratory proposal for schedule of financing and resources		
				1 year	2 year	3 year
Main items	Computers Electronic devices Materials		15 96 320	5 50 110	5 27 110	5 19 100
Resources	Hours	Design bureau DLNP Workshop	800 hours 1200 hours	300 500	300 500	200 200
Source of financing	Budget	Budget expenses (without salary)	587	217	194	176
	Non-budget	Grant of the Plenipotentiary of Georgia	30	10	10	10
		Program of the JINR-Belarus Cooperation.	15	5	5	5

Project leader **Z.Tsamalaidze**

Estimate of expenses for the project ″Search for coherent neutrino-less *μ -e* conversion at J-PARC (COMET) ″, 2017-2019

Form №29

NN	**Purpose of expenses from DLNP**	**Full cost**	**1st year**	**2nd year**	**3rd year**
	Direct expenses				
1.	Accelerator	-	-	-	-
2.	Computing	-	-	-	-
3.	Design bureau	800 hours	300	300	200
4.	Workshop LNP	1200 hours	500	500	200
5.	Materials	320k$	110	110	100
6.	Equipment	111k$	55	32	24
7.	Contracts for R&D	-	-	-	-
8.	Business trips:				
	a) To the non-rouble zone countries	150k$	50	50	50
	b) To the cities of rouble zone countries	6	2	2	2
	c) By protocols	-	-	-	-

Project leader **Z.Tsamalaidze**

Director of DLNP **V.A. Bednyakov**

Assistant director of DLNP on economics **G.A. Usova**